Computational Modelling and Topology-Aware Energy Flow Optimization in Spatial Nanosensor Networks

Artur Wilinski[1][0000−0002−3774−5909]

Warsaw University of Life Sciences - SGGW, Warsaw, Poland
artur.piotr.wilinski@gmail.com, artur_wilinski@sggw.edu.pl
Institute of Information Technology, Warsaw University of Life Sciences,
Warsaw, Poland, iit@sggw.edu.pl

Abstract. Modern intelligent nanosensor networks embedded in advanced IoT systems face fundamental challenges in energy efficiency and long-term autonomy. At the nanoscale, energy dissipation and connectivity depend on spatial topology and time-varying activity patterns. In this paper, we propose a unified computational framework for modeling and optimizing energy flow in spatial nanosensor networks using graph-based dynamics. Energy storage and leakage are modeled at each node using an equation of state. Inter-sensor couplings are represented by a weighted graph encoding the spatial connectivity and conductivity structure of the nanonetwork. We formulate a constrained dynamic optimization problem that minimizes a global energy functional over a finite horizon by adapting node-level activity (transmission/participation) and local computational intensity under physical and operational bounds. To preserve structural robustness, we enforce a spectral connectivity constraint via a penalty mechanism based on the algebraic connectivity of the Laplacian. We solve the resulting discretized problem using an iterative projected-gradient/SQP-type scheme (TOPENOPT) embedded in the network simulation loop. Computational experiments on ring and random geometric topologies demonstrate monotone decrease of the augmented objective, preservation of spectral connectivity above a prescribed threshold, reduction of localized dissipation bottlenecks, and predictable scalability with network size. These results confirm that topology-aware, spectrally constrained optimization enables energy-efficient sparsification of activity while maintaining global connectivity. Thereby, it lays the foundation for future adaptive and learning-based energy management in nanoscale IoT systems.

Keywords: nanosensor networks · energy flow modeling · topology-aware optimization · spectral connectivity

1 Introduction

Background and Motivation. Nanosensors used in IoT enable precise measurements at very small scales, but their tiny size severely limits energy storage

ICCS Camera Ready Version 2026
To cite this paper please use the final published version:
DOI: 10.1007/978-3-032-29909-3_26

and power availability. In dynamic and heterogeneous environments, managing energy becomes a key computational challenge that requires modeling both time dynamics and network topology. Inefficient energy distribution can quickly lead to node failures, reduced measurement quality, loss of connectivity, and ultimately failure of the entire network.

Key Challenges in Nanosensor Networks. Despite their potential, nanosensor networks face key energy optimization challenges that limit scalability, reliability, and long-term autonomy [1–3]. Energy losses from leakage, communication, processing, and inter-sensor couplings rapidly deplete limited resources. Furthermore, its stochastic nature complicates efficient storage and use. Spatial embedding further links connectivity to geometry, affecting topology and energy flow. Severe constraints in computation, memory, and bandwidth make energy-efficient communication difficult, requiring nanoscale optimal algorithms [4–6]. These challenges motivate dynamic, topology-aware optimization models addressing energy flow, storage, dissipation, and robustness [7–9].

Contribution of This Paper. This paper addresses the above challenges by proposing: (i) a unified node–network model of energy flow based on RC node dynamics coupled through a weighted graph Laplacian representing spatial conductance structure; (ii) a global energy functional that combines physical leakage losses with controllable processing/communication activity; (iii) a constrained dynamic optimization formulation that adapts node activation and computational intensity while preserving spectral connectivity using an algebraic-connectivity constraint; (iv) a penalty-based iterative numerical scheme embedded in the simulation loop (TOPENOPT); and (v) numerical validation on ring and random geometric topologies showing reduced dissipation hotspots, connectivity preservation, and predictable runtime scaling. The proposed framework contributes to the development of more sustainable and reliable nanosensor networks for biomedical, industrial [10] and IoT applications [11–13]. Existing power flow optimization methods cannot fully adapt to changing network topologies [14–16]. Current research deeply explores and proposes innovative topology-aware smart grid optimization frameworks.

2 Computational Model of Energy Flow in Nanosensor Networks

We develop a computational framework that links circuit-consistent node dynamics with graph-based coupling, providing a basis for topology-aware optimization. Throughout, nodes represent nanosensors and edges represent conductive couplings constrained by spatial geometry.

2.1 Circuit-Consistent Node Dynamics and Energy Accounting

From circuit law to Laplacian dynamics. Let $v_i(t)$ denote the voltage (energy-related state) at node i. Each node has capacitance C_i and leakage resistance

ICCS Camera Ready Version 2026
To cite this paper please use the final published version:
DOI: 10.1007/978-3-032-29909-3_26

$R_{eq,i}$. Neighbor couplings are modeled by conductances $G_{ij} \geq 0$. Using Kirchhoff's current law (KCL) at node i:

$$C_i \dot{v}_i(t) = i_{in,i}(t) - v_i(t) {R_{eq,i}}^{-1} - \sum_{j \in \mathcal{N}(i)} G_{ij}\big(v_i(t) - v_j(t)\big) - i_{proc,i}(t), \qquad (1)$$

where $i_{in,i}(t)$ is external injected current (e.g., harvesting or supply), and $i_{proc,i}(t)$ is an equivalent current draw capturing sensing/computation/communication load. Stacking voltages into $\mathbf{v}(t) \in R^N$ and letting $C = \mathrm{diag}(C_i)$, $R^{-1} = \mathrm{diag}(R_{eq,i}^{-1})$, and L_G be the weighted Laplacian induced by G_{ij}, we obtain:

$$C\dot{\mathbf{v}}(t) + \big(R^{-1} + L_G\big)\mathbf{v}(t) = \mathbf{i}_{in}(t) - \mathbf{i}_{proc}(t). \qquad (2)$$

In many computational experiments, $\mathbf{i}(t) := \mathbf{i}_{in}(t) - \mathbf{i}_{proc}(t)$ is treated as a net input, yielding the compact RC-on-graph form:

$$C\dot{\mathbf{v}}(t) + \tilde{L}_G\, \mathbf{v}(t) = \mathbf{i}(t), \qquad \tilde{L}_G := R^{-1} + L_G. \qquad (3)$$

Energy storage and dissipation. Energy stored at node i is $e_{store,i}(t) = \frac{1}{2} C_i v_i^2(t)$ and $p_{store,i}(t) = \dot{e}_{store,i}(t) = C_i v_i(t) \dot{v}_i(t)$. Leakage dissipation at node i is $p_{leak,i}(t) = v_i^2(t)/R_{eq,i}$.

Edge dissipation (Joule losses) and flow intensity. The current on edge (i, j) is $I_{ij}(t) = G_{ij}(v_i(t) - v_j(t))$. The *edge dissipation* (Joule loss) is

$$p_{edge,ij}(t) = \big(v_i(t) - v_j(t)\big) I_{ij}(t) = G_{ij}\big(v_i(t) - v_j(t)\big)^2. \qquad (4)$$

This quantity is a local dissipation indicator and for spatial edge-loss maps.

Communication load model. We model controllable communication power

$$p_{proc,i}(t) = \alpha_i\, n_i(t) + \beta_i\, u_i(t) + \gamma_i\, \delta_i(t) + \eta_i, \qquad (5)$$

at i-node, where $n_i(t)$ is the number of active incident connections, $u_i(t)$ is local computational intensity, $\delta_i(t) \in [0, 1]$ is a *continuous activation level* (soft duty-cycling / participation), and $\alpha_i, \beta_i, \gamma_i, \eta_i$ are coefficients. In the relaxed formulation used for optimization, δ_i is continuous; binarization may be applied post hoc if needed. In the proposed model, these variables $u_i(t)$ and $\delta_i(t)$ represent two different control mechanisms operating at different levels. The variable $\delta(t)$ controls the structural participation of nodes in the network. It modulates whether a node actively participates in communication and energy transfer, and thus directly affects the effective graph topology and the Laplacian matrix $\tilde{L}_G()$. It can be interpreted as a topology or activation control variable. In contrast, $u(t)$ represents the intensity of local computation performed at each node. It affects only the local processing power consumption term. Therefore, $\delta(t)$ governs network structure and connectivity, while $u(t)$ governs local computational load. Both are required to jointly optimize energy consumption and structural

ICCS Camera Ready Version 2026
To cite this paper please use the final published version:
DOI: 10.1007/978-3-032-29909-3_26

robustness. Next, we define the node-level cost indicator locally as leakage plus processing:

$$p_{tot,i}(t) = v_i^2(t) {R_{eq,i}}^{-1} + p_{proc,i}(t). \tag{6}$$

2.2 Global Objective and Constrained Optimization Problem

Global energy functional. Over a time horizon $[0, T]$, the global objective is

$$J(\mathbf{u}, \delta) = \int_0^T \sum_{i=1}^{N} \left(v_i^2(t) {R_{eq,i}}^{-1} + \alpha_i n_i(t) + \beta_i u_i(t) + \gamma_i \delta_i(t) + \eta_i \right) dt. \tag{7}$$

Dynamic constraint. According to the RC-on-graph dynamics

$$C\dot{\mathbf{v}}(t) + \tilde{L}_G(\delta(t))\, \mathbf{v}(t) = \mathbf{i}(t), \qquad \mathbf{v}(0) = \mathbf{v}_0. \tag{8}$$

the network state evolves. Here, $\tilde{L}_G(\delta)$ is the effective Laplacian built from activation-weighted conductances, e.g. $G_{ij}^{eff} = G_{ij} \min(\delta_i, \delta_j)$, which continuously attenuates edges incident to low-activity nodes.

Spectral connectivity constraint. To preserve structural robustness, we enforce a lower bound on algebraic connectivity:

$$\lambda_2\Big(\tilde{L}_G(\delta(t))\Big) \geq \lambda_{\min}, \qquad t \in [0, T], \tag{9}$$

where $\lambda_2(\cdot)$ is the second smallest Laplacian eigenvalue.

Control constraints. The control variables are subject to admissibility bounds reflecting physical limitations of the nodes. In particular, computational intensity and activation levels must remain within feasible ranges:

$$\mathbf{u}(t) \in \mathcal{U}, \qquad \delta(t) \in \mathcal{D} = [0, 1]^N, \qquad t \in [0, T]. \tag{10}$$

Here, $\mathbf{u}(t)$ represents local computational load, bounded by hardware capabilities, while $\delta(t)$ denotes continuous activation levels of nodes, where $\delta_i = 0$ corresponds to deactivation and $\delta_i = 1$ to full activity. These constraints ensure that the optimization remains physically realizable.

Constrained dynamic optimization. The energy management problem is formulated as a constrained optimal control problem. The objective is to minimize total energy consumption over the time horizon while satisfying the network dynamics, the spectral connectivity requirement, and the control bounds:

$$\min_{\mathbf{u}(\cdot),\, \delta(\cdot)} J(\mathbf{u}, \delta) \quad s.t. \quad (8),\ (9),\ (10). \tag{11}$$

The dynamic constraint enforces physical energy flow consistency, the connectivity constraint preserves structural robustness via $\lambda_2(L_G) \geq \lambda_{\min}$, and the control constraints guarantee feasibility of the optimized activation strategy.

ICCS Camera Ready Version 2026
To cite this paper please use the final published version:
DOI: 10.1007/978-3-032-29909-3_26

2.3 Numerical Solution: Time Discretization and Penalty-Based TOPENOPT

The continuous-time optimal control problem is solved via direct transcription, discretizing the dynamics and yielding a finite-dimensional nonlinear programming problem. The proposed topology-aware algorithm, TOPENOPT, iteratively alternates between simulation of network dynamics and projected optimization of control variables, enforcing the spectral connectivity constraint via a penalty mechanism. Starting with initialization (Step 1), each iteration simulates dynamics using (12) to obtain the state trajectory (Step 2), evaluates the augmented objective (energy + penalty) (Step 3), and updates controls via projected gradient or SQP (Step 4). If the spectral constraint is violated, the penalty or step size is adjusted (Step 5). The process continues until convergence and stabilization (Step 6).

Table 1. Iterative topology-aware energy optimization algorithm TOPENOPT

Step	Description
1	Initialize $\mathbf{u}^{(0)}[k]$, $\delta^{(0)}[k]$, set penalty $\rho > 0$, step size s_m.
2	Simulate network dynamics via (12) to obtain $\mathbf{v}^{(m)}[k]$.
3	Compute $J_\rho^{(m)} = J(\mathbf{u}^{(m)}, \delta^{(m)}) + \rho\Phi(\delta^{(m)})$.
4	Update controls using projected gradient / SQP step: $\mathbf{u}^{(m+1)} \leftarrow \Pi_{\mathcal{U}}\left(\mathbf{u}^{(m)} - s_m \nabla_{\mathbf{u}} J_\rho\right), \quad \delta^{(m+1)} \leftarrow \Pi_{\mathcal{D}}\left(\delta^{(m)} - s_m \nabla_{\delta} J_\rho\right).$
5	If $\min_k \lambda_2(\tilde{L}_G(\delta^{(m)}[k])) < \lambda_{\min}$, increase penalty $\rho \leftarrow \kappa\rho$, $\kappa > 1$ (or reduce s_m).
6	Repeat Steps 2–5 until convergence of J_ρ and stabilization of controls.

Discrete dynamics. The continuous time dynamics are discretized over a uniform time grid. Let $t_k = k\Delta t$, $k = 0, \ldots, K$, with $T = K\Delta t$. The state update reads

$$\mathbf{v}[k+1] = \mathbf{v}[k] + \Delta t\, C^{-1}\Big(\mathbf{i}[k] - \tilde{L}_G(\delta[k])\,\mathbf{v}[k]\Big). \tag{12}$$

This explicit scheme approximates the continuous RC network dynamics and transforms the differential constraint into a recursive state update suitable for numerical optimization.

Discrete objective. The continuous-time energy functional is approximated by the sum over the discrete time grid:

$$J = \sum_{k=0}^{K-1} \sum_{i=1}^{N} \left(\frac{v_i^2[k]}{R_{eq,i}} + \alpha_i n_i[k] + \beta_i u_i[k] + \gamma_i \delta_i[k] + \eta_i \right) \Delta t. \tag{13}$$

This expression represents the total accumulated energy consumption over the horizon $[0, T]$, including physical dissipation and controllable processing activity.

ICCS Camera Ready Version 2026
To cite this paper please use the final published version:
DOI: 10.1007/978-3-032-29909-3_26

Penalty for connectivity violations. To enforce the spectral connectivity requirement in the discretized setting, a quadratic penalty is introduced:

$$\Phi = \sum_{k=0}^{K-1} \left[\max\left(0,\ \lambda_{\min} - \lambda_2\Big(\tilde{L}_G(\delta[k])\Big)\right)\right]^2. \tag{14}$$

The term Φ penalizes any violation of the algebraic connectivity constraint at each time step. The augmented objective function is defined as $J_\rho = J + \rho\Phi$ ($\rho > 0$), where ρ controls the strength of constraint enforcement. This formulation converts the constrained optimal control problem into a finite-dimensional nonlinear optimization problem suitable for iterative numerical solution. The relaxation $\delta \in [0,1]^N$ yields a continuous sparsification model compatible with gradient-based updates. If a binary schedule is required, δ_i can be thresholded after convergence, followed by a short repair step to restore $\lambda_2 \geq \lambda_{\min}$.

Spectral identification of least-critical nodes (optional analysis). Let $\tilde{L}_G \in R^{N\times N}$ denote the effective Laplacian. The algebraic connectivity is $\lambda_2(\tilde{L}_G)$ with eigenvector $\mathbf{f}$ satisfying $\tilde{L}_G\mathbf{f} = \lambda_2(\tilde{L}_G)\mathbf{f}$. A practical local criticality proxy is

$$\kappa_i \approx \sum_{j\in\mathcal{N}(i)} G_{ij}^{eff}\,(f_i - f_j)^2, \tag{15}$$

where $G_{ij}^{eff} = G_{ij}\min(\delta_i, \delta_j)$. Nodes with small κ_i tend to have limited first-order impact on λ_2 when weakened, hence they are natural candidates for reducing δ_i within the optimization loop.

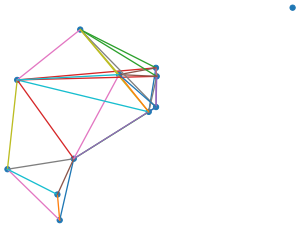

Fig. 1. Spatially embedded nanosensor network as a graph. Nodes are spatially distributed nanosensors; edges are couplings constrained by geometry.

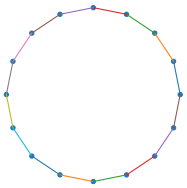

Fig. 2. Spatially embedded ring topology used as a structured baseline.

The spatial structure of the nanosensor network is illustrated in Fig. 1, where nodes represent spatially distributed sensors and edges correspond to geometry-constrained interactions. This representation emphasizes how spatial embedding

ICCS Camera Ready Version 2026
To cite this paper please use the final published version:
DOI: 10.1007/978-3-032-29909-3_26

determines feasible communication links and energy transfer paths. For comparison, a structured baseline topology is shown in Fig. 2. The ring graph provides a regular connectivity pattern with uniform node degree, which serves as a reference case for analyzing the impact of topology on energy flow optimization and spectral properties. In particular, such structured topologies typically exhibit more stable algebraic connectivity λ_2, whereas irregular spatial graphs may experience larger variations, which directly affects robustness and the feasibility of activity reduction under the constraint $\lambda_2(L_G) \geq \lambda_{\min}$.

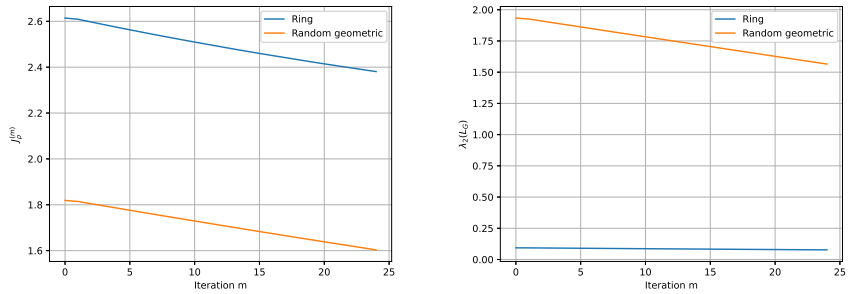

Fig. 3. Numerical performance of the proposed spectrally constrained optimization. Left: convergence of augmented objective function J_ρ versus iteration number. Right: evolution of algebraic connectivity $\lambda_2(\tilde{L}_G)$ versus iteration number.

The numerical behavior of the proposed optimization framework is illustrated in Fig. 3. The left plot shows the convergence of the augmented objective function J_ρ as a function of the iteration index m. For both topologies, the objective decreases monotonically, indicating stable convergence of the optimization algorithm. The ring topology starts at a higher value (approximately 2.6) and decreases gradually to about 2.4, whereas the random geometric topology starts lower (around 1.8) and decreases to approximately 1.6. The nearly linear and smooth decrease in both cases indicates steady improvement without instability. The higher initial value of J_ρ for the ring topology is due to initial conditions and limited energy dissipation paths, rather than the topology itself. The comparison focuses on the convergence behavior and relative reduction of the objective. The right plot presents the evolution of algebraic connectivity $\lambda_2(\tilde{L}_G)$ versus the iteration index. The random geometric graph exhibits high initial connectivity (around 2.0), which gradually decreases to about 1.6 as the optimization reduces redundant connections and activity. In contrast, the ring topology has low but stable connectivity (around 0.1), reflecting its sparse and regular structure. Importantly, in both cases λ_2 remains above zero, indicating that the network stays connected throughout the optimization process. These results show that the algorithm consistently reduces energy consumption while preserving network

ICCS Camera Ready Version 2026
To cite this paper please use the final published version:
DOI: 10.1007/978-3-032-29909-3_26

connectivity. The decrease in λ_2 for the random topology reflects controlled sparsification rather than loss of connectivity, whereas the stability of λ_2 in the ring case confirms robustness of networks under optimization.

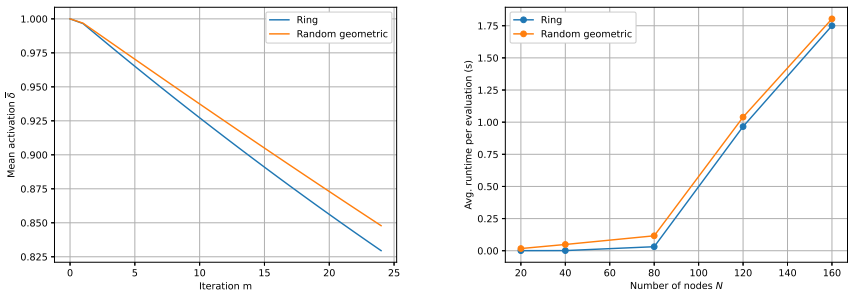

Fig. 4. Numerical performance of the proposed spectrally constrained optimization. Left: mean activation $\overline{\delta}$ (soft sparsification) versus iteration number. Right: scalability measured as average runtime per objective evaluation versus network size N.

The numerical performance of the proposed optimization framework for mean activation and scalability is illustrated in Fig. 4. The left plot shows the evolution of the mean node activation level $\overline{\delta}$ as a function of the iteration index m. In both topologies, $\overline{\delta}$ decreases almost linearly from the initial fully active state ($\overline{\delta} \approx 1$), indicating gradual sparsification of node activity during optimization. The ring topology achieves slightly lower final activation (≈ 0.83 vs. ≈ 0.85), as its regular structure allows connectivity to be preserved with fewer active nodes. In contrast, the random geometric graph requires higher residual activation due to irregular connectivity. The right plot illustrates scalability. The horizontal axis shows network size N, and the vertical axis represents average runtime per objective evaluation. Runtime increases with N, with a more pronounced growth for larger networks ($N \geq 80$), reflecting the cost of matrix operations and spectral evaluations.The random topology consistently requires slightly higher runtime due to its less structured Laplacian. The method reduces node activity while preserving connectivity and predictable computational scaling. These trends are consistent with Table 2, where the ring topology shows lower activation and slightly better energy reduction, while the random graph requires higher activation and incurs higher computational cost. The spatial distribution of edge dissipation is shown in Fig. 5. The plots are embedded in physical space; therefore, there are no traditional Cartesian axes. Node positions correspond to spatial coordinates, while edges represent connections between sensors. The color scale and line thickness encode the magnitude of edge dissipation $p_{edge,ij} = G_{ij}(v_i - v_j)^2$. The left plot (before optimization) exhibits several high-intensity edges (bright and thick lines), indicating localized dissipation hotspots caused by large volt-

ICCS Camera Ready Version 2026
To cite this paper please use the final published version:
DOI: 10.1007/978-3-032-29909-3_26

age differences between connected nodes. These regions correspond to inefficient energy transfer and concentration of losses. The right plot (after optimization) shows a more uniform distribution of edge dissipation. High-intensity edges are significantly reduced, and energy flow is redistributed across the network. This indicates that the optimization mitigates local bottlenecks while maintaining global connectivity. Importantly, this redistribution is achieved under the constraint $\lambda_2(L_G) \geq \lambda_{\min}$, ensuring that the reduction of local dissipation does not compromise structural connectivity.

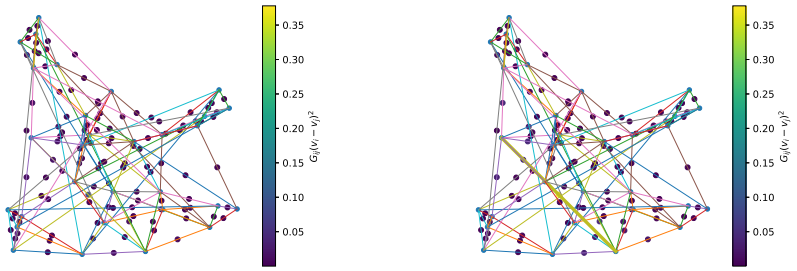

Fig. 5. Spatial edge-dissipation maps before (left) and after (right) optimization for the same topology. Edge dissipation is quantified by $p_{edge,ij} = G_{ij}(v_i - v_j)^2$. Reduced thick/high-intensity edges indicate mitigation of local dissipation bottlenecks under the connectivity constraint.

Fig. 6. Edge-dissipation redistribution in a 10-node network before (left) and after (right) optimization. Edge thickness is proportional to $p_{edge,ij} = G_{ij}(v_i - v_j)^2$. The underlying topology is unchanged; effective activity attenuates couplings continuously.

The algebraic connectivity remains positive, confirming that energy smoothing is obtained without fragmenting the network. The proposed method smooths

ICCS Camera Ready Version 2026
To cite this paper please use the final published version:
DOI: 10.1007/978-3-032-29909-3_26

energy gradients, reduces peak dissipation, and improves efficiency while preserving spectral robustness. A detailed view of edge-dissipation redistribution is shown in Fig. 6. The plots are embedded in physical space and do not use explicit Cartesian axes; node positions represent spatial locations, while edges correspond to connections between sensors. Edge thickness encodes the magnitude of dissipation $p_{edge,ij} = G_{ij}(v_i - v_j)^2$. The left plot (before optimization) reveals several dominant edges with higher thickness, indicating localized dissipation concentrated along specific links. These correspond to uneven energy gradients and inefficient load distribution across the network. The right plot (after optimization) shows a clear redistribution of dissipation. Thick edges are reduced and energy flow becomes more balanced across the network. Importantly, the underlying topology remains unchanged, and the effect is achieved through continuous modulation of node activity. Consistent with Fig. 5, this result confirms that the proposed optimization smooths local energy imbalances and mitigates dissipation hotspots while preserving structural connectivity under the spectral constraint. This demonstrates that local adjustments of node activity lead to a globally improved energy distribution, highlighting the interplay between local control actions and global network behavior. Fig. 7 illustrates the effect of soft sparsification with partially deactivated nodes. The network is embedded in physical space (no explicit Cartesian axes), where node positions correspond to spatial locations. Node size encodes the activation level $\delta_i \in [0, 1]$, while edge thickness represents dissipation $p_{edge,ij} = G_{ij}(v_i - v_j)^2$.

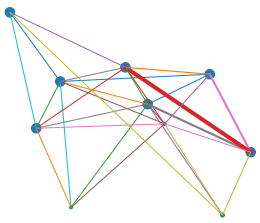

Fig. 7. Soft sparsification with partially deactivated nodes. Node size is proportional to activation $\delta_i \in [0, 1]$, while edge thickness represents edge dissipation $p_{edge,ij} = G_{ij}(v_i - v_j)^2$. Despite local deactivation, spectral connectivity is preserved ($\lambda_2(\tilde{L}_G) \geq \lambda_{\min}$).

In contrast to Fig. 5 and Fig. 6, where all nodes are active, this figure shows that some nodes are significantly attenuated (small node size), indicating reduced participation in energy transfer. As a result, adjacent edges become thinner, reflecting lower local dissipation and reduced energy flow through less critical parts of the network. Importantly, despite this local deactivation, the network remains globally connected, as indicated by the condition $\lambda_2(\tilde{L}_G) \geq \lambda_{\min}$. This demonstrates that the optimization identifies and suppresses non-critical nodes while

ICCS Camera Ready Version 2026
To cite this paper please use the final published version:
DOI: 10.1007/978-3-032-29909-3_26

preserving the structural backbone of the network. Compared to previous figures, this example highlights a stronger form of optimization: not only is dissipation redistributed, but the network is also selectively sparsified. This confirms that the proposed method can reduce energy usage by deactivating redundant nodes, while maintaining global robustness and connectivity. From an IoT perspective, such controlled sparsification directly translates into extended network lifetime and improved energy efficiency without compromising system functionality.

3 Results

Experimental Setup. We evaluate the proposed framework on (i) a ring topology and (ii) a random geometric graph generated by uniformly sampling node positions in $[0,1]^2$ and connecting nodes within a distance threshold r (see Fig. 1–2). All simulations use horizon T, time step Δt, and $K = T/\Delta t$ steps. Capacitances C_i, leakage resistances $R_{eq,i}$, and base conductances G_{ij} are fixed physical parameters; activation $\delta_i[k] \in [0,1]$ continuously attenuates effective couplings $G_{ij}^{eff}[k]$. The connectivity threshold is $\lambda_{\min}$. TOPENOPT is run with initial penalty ρ_0, growth factor κ, and step size schedule s_m.

Convergence and Connectivity Preservation. Figure 3 shows monotone decrease of the augmented objective J_ρ for both topologies, confirming stable convergence of TOPENOPT under the penalty enforcement of (9). The algebraic connectivity $\lambda_2(\tilde{L}_G)$ remains above the threshold $\lambda_{\min}$ throughout iterations, demonstrating that energy-efficient sparsification does not compromise global connectivity. The ring topology exhibits smoother λ_2 evolution due to its regular structure, while the random geometric topology shows stronger early variations that stabilize as the penalty term guides the iterates back into the feasible connectivity region.

Soft Sparsification and Activity Reduction. Figure 4 presents the evolution of mean activation $\overline{\delta}$. In the ring case, $\overline{\delta}$ decreases gradually and stabilizes at a lower level, indicating that the structured topology supports stronger activity reduction while maintaining the spectral constraint. For random graphs, $\overline{\delta}$ stabilizes at a slightly higher level, reflecting the need to keep more nodes/links active to preserve $\lambda_2(\tilde{L}_G) \geq \lambda_{\min}$ under irregular spatial connectivity.

Scalability. Figure 4 reports average runtime per objective evaluation versus network size N. Runtime increases with N for both topologies, reflecting the cost of state simulation and repeated spectral evaluations of λ_2. Random geometric graphs exhibit higher runtime due to increased edge density and less regular sparsity patterns in $\tilde{L}_G$, which increases the cost of matrix operations and eigenpair computations.

Spatial Redistribution of Dissipation. Figure 5 visualizes the spatial distribution of edge dissipation $p_{edge,ij} = G_{ij}(v_i - v_j)^2$ before and after optimization. Post-optimization maps show attenuation of high-loss edges, indicating mitigation of localized bottlenecks while preserving connectivity. Figure 6 provides a compact illustration for $N = 10$, confirming that dissipation is redistributed

ICCS Camera Ready Version 2026
To cite this paper please use the final published version:
DOI: 10.1007/978-3-032-29909-3_26

without changing the underlying topology, but through continuous activity-dependent attenuation of effective couplings.

Partial Deactivation Case Study. Figure 7 demonstrates a configuration with near-deactivated nodes ($\delta_i \approx 0$ for selected nodes), representing strong duty-cycling. Despite local suppression, the network remains spectrally connected and satisfies $\lambda_2(\tilde{L}_G) \geq \lambda_{\min}$.

Summary of Quantitative Results. Table 2 summarizes the quantitative outcomes of the proposed topology-aware optimization framework for structured (ring) and irregular (random geometric) spatial topologies. Although only two representative cases are shown, they capture fundamentally different connectivity regimes. The ring topology achieves higher energy reduction (21.5% vs. 18.5%) and lower final activation ($\overline{\delta}_{final} = 0.57$ vs. 0.64). This difference is primarily structural rather than algorithmic. In the ring topology, connectivity is uniformly distributed, allowing more uniform and aggressive reduction of node activity without violating the spectral constraint. In contrast, the random geometric graph exhibits heterogeneous connectivity, where certain nodes are more critical for maintaining λ_2. As a result, the feasible reduction of activation is more limited, requiring higher residual activity and leading to slightly lower energy savings. The minimum values of λ_2 remain close to the threshold $\lambda_{\min} = 0.15$ in both cases, indicating that the optimization operates near the boundary of the feasible region. This confirms that the spectral constraint actively shapes the solution and limits sparsification. The optimization reduced total energy dissipation by approximately 20% in both topologies. Before optimization, many nodes remained active despite limited structural importance.

Table 2. Quantitative comparison of optimization results for ring and random geometric topologies ($N = 80$, $\lambda_{\min} = 0.15$).

Topology	J_{before}	J_{after}	ΔJ (%)	$\min \lambda_2$	$\overline{\delta}_{final}$
Ring	13.52	10.61	21.5%	0.158	0.57
Random Geometric	14.08	11.48	18.5%	0.151	0.64

After optimization, node activity was reduced while maintaining the spectral constraint $\lambda_2(L_G) \geq \lambda_{\min}$. Overall, the results demonstrate that topology determines the achievable trade-off between energy efficiency and connectivity. The observed differences arise from the topology-dependent feasibility region imposed by the spectral constraint, rather than from differences in the optimization procedure itself. The final mean activation $\overline{\delta}_{final}$ reflects the degree of achievable sparsification under the spectral constraint. The ring topology reaches a lower activation level (0.57) compared to the random geometric graph (0.64), indicating that a larger portion of nodes can be deactivated without violating connectivity. This difference is a direct consequence of topology. In the ring, connectivity is uniformly distributed, allowing activity reduction to be applied more evenly across nodes. In contrast, the random geometric graph contains structurally

ICCS Camera Ready Version 2026
To cite this paper please use the final published version:
DOI: 10.1007/978-3-032-29909-3_26

critical nodes that must remain active to preserve $\lambda_2(L_G) \geq \lambda_{\min}$, which limits sparsification. Thus, $\overline{\delta}_{final}$ provides a quantitative measure of how strongly the network can be energy-optimized under connectivity constraints.

Convergence and Stopping Criteria. The results reported in Table 2 were obtained using a direct transcription approach with explicit time discretization of the continuous-time optimal control problem. The iterative optimization procedure (TOPENOPT) was terminated according to the following criteria:
Objective stabilization. The relative decrease of the augmented objective function (objective stabilization refers to the relative decrease of the augmented objective function J_ρ, which combines the physical energy cost and the penalty enforcing the spectral connectivity constraint).

$$\frac{|J_\rho^{(m)} - J_\rho^{(m-1)}|}{\max\{1, |J_\rho^{(m-1)}|\}} < 10^{-4}.$$

Control stabilization. The relative change of control trajectories fulfilled

$$\frac{\|\mathbf{u}^{(m)} - \mathbf{u}^{(m-1)}\|_2}{\max\{1, \|\mathbf{u}^{(m-1)}\|_2\}} < 10^{-3}, \quad \frac{\|\delta^{(m)} - \delta^{(m-1)}\|_2}{\max\{1, \|\delta^{(m-1)}\|_2\}} < 10^{-3}.$$

Connectivity feasibility. The spectral constraint was satisfied within tolerance,

$$\min_k \left(\lambda_2(\tilde{L}_G(\delta[k])) - \lambda_{\min}\right) \geq -10^{-3}.$$

These criteria ensure numerical stability and approximate first-order stationarity. The spectral coherence constraint is met within tolerance. The exact number of iterations depends on the network topology and initialization. In our experiments, convergence was typically achieved within 30–60 iterations for networks up to N $\approx$ 100, confirming computational feasibility. In particular, structured topologies (e.g., ring-shaped) tend to converge faster, while random geometric graphs may require more iterations due to higher connectivity variability and stronger activation adjustments. The results show that topology-aware spectral constraints reduce global energy dissipation while preserving structural robustness. Ring topologies allow stronger activity sparsification, reflected in lower final mean activation $\overline{\delta}_{final}$. Random geometric graphs require higher residual activation to maintain connectivity. The near-threshold values of $\min \lambda_2$ confirm effective enforcement of the robustness constraint. Runtime grows predictably with network size, indicating scalability for moderately large networks.

4 Discussion

Energy dissipation in nanosensor networks strongly depends on spatial topology and coupling. Structured topologies (e.g., ring) maintain stable connectivity and allow greater activity reduction without violating $\lambda_2(\tilde{L}_G) \geq \lambda_{\min}$, while irregular graphs require adaptive corrections guided by a penalty mechanism.

ICCS Camera Ready Version 2026
To cite this paper please use the final published version:
DOI: 10.1007/978-3-032-29909-3_26

Spectral Constraint. Algebraic connectivity λ_2 serves as a proxy for robustness: $\lambda_2 > 0$ ensures connectivity, and higher values improve resilience. The constraint prevents energy savings at the cost of network disconnection (9), though it does not capture all effects (e.g., delays or interference).
Soft Sparsification. The relaxed activation variable $\delta \in [0,1]^N$ enables smooth, gradient-based reduction of activity while preserving connectivity. This continuous model is compatible with gradient-based optimization and enables controlled reduction of activity while preserving connectivity. If binary schedules are required, thresholding and feasibility repair can be applied after convergence.
Limitations and scalability. The RC-based model simplifies energy and communication dynamics and omits stochastic channel effects. Scalability is limited by repeated evaluation of λ_2. This framework can be extended by including stochastic terms and probabilistic communication costs. From a computational perspective, multiple algebraic connectivity evaluation introduces additional costs for larger networks.
Outlook. Future work includes extensions to time-varying geometries, stochastic models, and data-driven methods (e.g., reinforcement learning), as well as multi-physics coupling for smart materials and biomedical sensing.

5 Conclusions

This work addresses energy-efficient operation in spatial nanosensor networks under strict power constraints and topology-dependent losses. We introduced an RC-on-graph modeling framework combined with a topology-aware optimization algorithm (TOPENOPT), which adapts node activation while enforcing a spectral connectivity constraint.

Numerical results for ring and random geometric topologies show about a 20% reduction in total energy dissipation while maintaining algebraic connectivity above the required threshold. The optimization mitigates localized dissipation hotspots and enables controlled sparsification of node activity without loss of global robustness. Regular ring topologies permit stronger activity reduction with lower final mean activation, whereas irregular graphs require higher residual activity to satisfy connectivity constraints. The direct-transcription approach ensures stable convergence under well-defined stopping criteria, with predictable scaling of execution time as network size increases. These results demonstrate that spectrally constrained optimization is a computationally efficient and robust strategy for power management in nanoscale IoT systems. The framework formulates energy management as a computational problem on dynamic graphs, integrating graph theory, constrained nonlinear optimization, and algorithm design under limited resources. Operating on sparse structures with enforced spectral constraints, it aligns with key areas of computer science, particularly distributed and energy-aware systems.

Future work will focus on learning-based control, where the constraint $\lambda_2(L_G) \geq \lambda_{\min}$ can be incorporated into reinforcement learning as a safety condition, via penalty terms or constrained RL formulations, enabling adaptive policies that

ICCS Camera Ready Version 2026
To cite this paper please use the final published version:
DOI: 10.1007/978-3-032-29909-3_26

preserve network connectivity during operation. In this setting, the RL agent learns adaptive activation policies while preserving spectral robustness of the network during exploration.

Disclosure of Interests. The author reports no conflicts of interest related to the content of this article.

References

1. Zheng, F., Lingji, K. et al.: A multi-node self-powered fault detection system by triboelectric-electromagnetic nanosensors for smart transportation. Nano Energy **128**(A), 109882, (2024)
2. Ting, Y., Yinan, G. et al.: Dynamic energy flow optimization of electricity and hydrogen-enriched natural gas integrated energy systems. International Journal of Hydrogen Energy **109**, 1274–1285, (2025)
3. Aleem, A., Thumma, R.: Optimizing Energy Efficiency in IoT-Enabled Wireless Sensor Networks Using an Integrated EEKA-K-means Approach. Int. J. of Intelligent Engineering and Systems **18**(2), (2025)
4. Njah, Y., Cheriet, M.: Parallel Route Optimization and Service Assurance in Energy-Efficient Software-Defined Industrial IoT Networks. IEEE Access **9**, 24682–24696, (2021)
5. Chen, Z., Sivaparthipan, C.: IoT based smart and intelligent smart city energy optimization. Sustainable Energy Techn. and Assessments **49**, 101724, (2022)
6. Hamrouni, A., Pollin, S., Sallouha, H.: Resource Allocation in Hybrid Radio-Optical IoT Networks using GNN with Multi-task Learning. IEEE Transactions on Machine Learning in Communications and Networking, arXiv:2511.07428 (2026)
7. Zhu, C., Byrd H. et al.: L-BFGS-B: Algorithm 778: L-BFGS-B, FORTRAN routines for large scale bound constrained optimization". ACM Transactions on Mathematical Software **23**(4), 550––560 (1997)
8. Mokhtari, A., Ribeiro, A.: Global convergence of online limited memory BFGS. Journal of Machine Learning Research **16**, 3151––3181 (2015)
9. Alabdulatif, A., Thilakarathne, N.N., Lawal, Z.K. et al.: Internet of Nano-Things (IoNT): A Comprehensive Review from Architecture to Security and Privacy Challenges. Sensors **23**(5), 2807, (2023)
10. Khan, M.N., Ullah, I. et al.: Reinforcement Learning-Based Dynamic Power Management for Energy Optimization in IoT-Enabled Consumer Electronics. IEEE Transactions on Consumer Electronics **71**(3), (2025)
11. Xu, J., Xin, L. et al.: Energy harvesting-based thermal aware routing protocol for lung terahertz nanosensor networks. Nano Communic. Networks **43**, 100563, (2025)
12. Wilinski, A., El Fray, I.: Skin sensors modelling for smarter and safer autonomous systems. ASTRJ **19**, 362–380, (2025)
13. El Fray, I., Wilinski, A.: Modifications of the Formal Risk Analysis and Assessment for the Information System Security. ASTRJ **18**(2), 317–332, (2024)
14. Wang, K., Jiang, K., et al.: Research on topology-aware power flow optimization and load forecasting model of smart grid. Microchem. J. **218**, 115046, (2025)
15. Reddy, Y.M., Raj, V. H., et al.: Topology-Aware Optimal Power Flow Solutions Using Reinforcement Learning, Int. Conf. on Power Energy, Environment and Intelligent Control (PEEIC), 1736–1740, (2023)
16. Ding, Z., Shen, L., Chen, H. et al.: Energy-Efficient Topology Control Mechanism for IoT-Oriented Software-Defined WSNs. IEEE IoT Journal **10**(15), (2023)

ICCS Camera Ready Version 2026
To cite this paper please use the final published version:
DOI: 10.1007/978-3-032-29909-3_26